Journal of Nuclear Materials 381 (2008) 231–241

Contents lists available at ScienceDirect

Journal of Nuclear Materials

journal homepage: www.elsevier.com/locate/jnucmat

Probabilistic methodology to estimate environmental conditions for localized corrosion and stress corrosion cracking of Alloy 22 in a high-level radioactive waste repository setting

Osvaldo Pensado *, Roberto Pabalan

Center for Nuclear Waste Regulatory Analyses (CNWRA), 6220 Culebra Road, San Antonio, TX 78238, USA

ARTICLE INFO

Article history:
Received 16 November 2007
Accepted 18 August 2008

ABSTRACT

The US Department of Energy (DOE) has indicated that it may use Alloy 22 (Ni–22Cr–13Mo–4Fe–3W) as the waste package outer container material for the potential high-level waste repository at Yucca Mountain, Nevada. This alloy could be susceptible to localized corrosion, in the form of crevice corrosion, and stress corrosion cracking if environmental conditions and material requirements (e.g., existence of crevices or high enough tensile stresses) are met. An approach is proposed to assess the likelihood of environmental conditions capable of inducing crevice corrosion or stress corrosion cracking in Alloy 22. The approach is based on thermodynamic simulations of evaporation of porewaters and published equations to compute corrosion potential and critical potentials for crevice corrosion and stress corrosion cracking as functions of pH, ionic concentration, temperature, and metallurgical states from fabrication processes. Examples are presented to show how the approach can be used in system-level assessment of repository performance.

1. Introduction

The US Department of Energy (DOE) has indicated that for the potential high-level waste repository at Yucca Mountain, Nevada, the waste package may consist of an outer container made of Alloy 22 for corrosion resistance and an inner container made of Type 316 nuclear grade stainless steel for structural support [1]. The waste package is proposed to be protected against seepage water and rockfall arising from gradual degradation of drifts by an independent titanium alloy structure referred to as 'drip shield' [1]. Radioactive decay can cause waste packages to experience transient temperatures well above the boiling point of pure water for several hundreds to few thousands of years. Deliquescent multicomponent salt systems have been reported that can form liquid solutions at temperatures as high as 200 °C or above [2]. In principle, those solutions can support electrochemical corrosion processes. Feasible rates of corrosion of Alloy 22 at those elevated temperatures are currently being investigated by other authors. Localized corrosion, in the form of crevice corrosion (CC), and stress corrosion cracking (SCC) of Alloy 22 have been observed in tests conducted in aqueous solutions at temperatures lower than 110 °C [3–6]. Appropriate environmental conditions (water compositions and temperature) must be established for the initiation and propagation of CC or SCC. If those conditions are not established, Alloy 22 is expected to undergo passive dissolution at corrosion rates less than 100 nm/yr [1,3].

The environmental requirements for CC and SCC have been delineated elsewhere [3–9]. Crevice corrosion of Alloy 22 is feasible if (i) tight crevices form, (ii) concentrated chloride solutions are available with low concentrations of oxyanions (nitrate, carbonate/bicarbonate, sulfate) capable of inhibiting CC, and (iii) high enough corrosion potentials are attained [3–5,7,8]. Stress corrosion cracking of Alloy 22 has been observed in bicarbonate solutions containing sufficient concentration of chloride ions at temperatures above 60 °C using slow strain rate tests with tensile samples polarized at high anodic potentials [6,9]. Therefore, SCC of Alloy 22 appears feasible if (i) the material is affected by high tensile stresses, (ii) solutions are available with enough concentrations of chloride and bicarbonate, and (iii) high enough corrosion potentials are attained [6,9].

The concentrated solutions required for both CC and SCC could form on the waste package by evaporation of seepage water. If seepage does not contact the waste package surface, another source for the formation of aqueous solutions is moisture in the environment. Analyses of dusts gathered in the Yucca Mountain region reveal that sulfate and nitrate are dominant salt components [10,11]. Solutions arising from deliquescence of salts in dust or by mixing of salts with condensed water are envisioned to contain high nitrate concentration to possibly inhibit Alloy 22 crevice corrosion [2]. The question of whether deliquescence solutions can support localized corrosion of Alloy 22 is under investigation. This paper focuses on the scenario where seepage water contacts the

* Corresponding author. Tel.: +1 210 522 6084; fax: +1 210 522 6081.
E-mail address: opensado@swri.org (O. Pensado).

0022-3115/$ - see front matter © 2008 Elsevier B.V. All rights reserved.
doi:10.1016/j.jnucmat.2008.08.002

waste package. An approach is proposed to assess the likelihood of environmental conditions capable of supporting initiation and propagation of CC or SCC in Alloy 22 under the 'waste package seepage contact' scenario. The approach accounts for variability in solution composition, variation in temperature, and the different susceptibilities of mill-annealed and weld zones to CC. The methodology is proposed to be used in system-level assessment of repository performance. Assessment of additional requirements for CC and SCC, such as formation of crevices or development of regions of sufficiently high tensile (residual or applied) stresses, is discussed only at a qualitative level to complement performance assessments.

2. Mathematical approach

2.1. Critical potentials and corrosion potential

The approach for classifying solution compositions as capable of supporting (i.e., initiating and propagating) CC or SCC is based on comparison of the corrosion potential, E_{corr}, to a critical potential, E_{crit}. Thus, for a particular solution composition, if the corrosion potential, E_{corr}, exceeds a critical potential, E_{crit}, the solution is considered capable of promoting a detrimental corrosion mode (CC or SCC).

The critical potential for CC is defined in this paper as the crevice corrosion repassivation potential, E_{rcrev}. It is assumed that, in the long term, E_{rcrev} is the lowest potential at which active crevice corrosion can be initiated and propagated [12]. E_{rcrev} is a function of the temperature, solution composition, and fabrication states (e.g., welded and mill-annealed Alloy 22) [3–5]. The repassivation potential decreases with increasing chloride concentration and significantly increases if oxyanions such as nitrate, bicarbonate, and sulfate are present in the solution [8]. Dunn et al. [3–5] published an empirical relationship for mill-annealed and thermally aged material defining E_{rcrev} as a function of temperature, chloride concentration, and oxyanion concentrations:

$$E_{rcrev}(T) = A_1 + A_2 T + (B_1 + B_2 T)\log_{10}\left(\frac{[Cl^-]}{1\,mol/L}\right) + 0.8V \times \frac{\min(r_t, r_n)}{r_n} + \Delta E_{rcrev}, \quad (1)$$

where T is the absolute system temperature; A_1, A_2, B_1, B_2, and r_n are empirical parameters; ΔE_{rcrev} is an uncertainty term; and r_t is a linear combination of oxyanion-to-chloride concentration ratios defined as [3,5,8]:

$$r_t = \frac{[NO_3^-]}{[Cl^-]} + \frac{r_n}{r_s}\frac{[SO_4^{2-}]}{[Cl^-]} + \frac{r_n}{r_c}\frac{[CO_3^{2-}] + [HCO_3^-]}{[Cl^-]}. \quad (2)$$

The terms r_s and r_c are empirical parameters. The anion concentrations in Eqs. (1) and (2) are in units of mol/L. Values for the parameters for two material states, mill-annealed and thermally aged, are listed in Table 1. The E_{rcrev} is in units of Volts versus standard hydrogen electrode (V_{SHE}). The E_{rcrev} of the thermally aged material defines a lower bound to E_{rcrev} measured in welded samples [5,8]. Anderko et al. [13] developed a model to compute the repassivation potential of alloys in multicomponent electrolyte systems, accounting for aggressive species such as chloride and inhibiting species such as nitrate. The model accurately predicted the repassivation potential in a number of Fe–Ni–Cr–Mo alloys. The equations by Dunn et al. [3–5] are consistent with the Anderko et al. expressions.

For the current analysis, the published equation by Dunn et al. [3] was modified by the consideration of an uncertainty term, ΔE_{rcrev}, that spans 100 mV for thermally aged material and 310 mV for mill-annealed material (the parameters to compute E_{rcrev} according to Dunn et al. [3] correspond to median values in the present analysis). The 310 mV uncertainty interval was derived via confidence bounds in curve-fitting parameters. The values of E_{rcrev} for thermally aged material in general represent a lower bound for the weld material E_{rcrev}. For this reason, a narrower uncertainty envelope, 100 mV wide, was considered for thermally aged material. The uncertainty intervals are assumed constant (i.e., independent of temperature and solution compositions). The distribution functions for ΔE_{rcrev} are defined in Table 1.

Table 1
Parameters for the computation of the repassivation potential, E_{rcrev}, as a function of temperature and concentration of ionic species [3]

Parameter	Value, mill-annealed material	Value, thermally aged material
A_1 (V_{SHE})[a]	3.73	3.82
A_2 (V/K)	−0.0094	−0.01
B_1 (V)	−2.17	−1.59
B_2 (V/K)	0.0052	0.0037
r_n	0.1	0.3
r_s	0.5	0.5
r_c	0.2	0.2
ΔE_{rcrev} (V)	Triangular distribution function with the maximum (mode) at 0 and extremes at −0.155 and 0.155.	Triangular distribution function with mode at 0 and extremes at −0.05 and 0.05.

[a] V_{SHE}: Volts versus standard hydrogen electrode.

To study SCC, Chiang et al. [6] conducted slow strain rate tests selectively removing constituent anionic species (e.g., nitrate, sulfate, fluoride, or chloride) from a solution known to induce SCC to isolate the main ions causing SCC. A synergistic effect was discovered between bicarbonate and chloride ions in SCC of Alloy 22. At a constant bicarbonate level, the susceptibility of Alloy 22 to SCC increases with increasing chloride ion concentration. In pure bicarbonate or chloride solutions, no SCC was observed [6]. At fixed chloride and bicarbonate concentrations, SCC was only observed in alloy samples at high anodic polarization potentials. A critical potential, E_{SCC}, was inferred from the experimental database by analyzing the lowest anodic polarization potentials required to induce SCC [3,9]. As a first approximation, Shukla et al. [9] proposed a linear equation to compute E_{SCC} as a function of temperature:

$$E_{SCC}(T) = 2.11V_{SHE} - 4.62\times10^{-3}T\ V/K + \Delta E_{SCC}, \quad (3)$$

where ΔE_{SCC} is an uncertainty term. In this paper, the uncertainty term was sampled from a triangular probability distribution function with the maximum (mode) at 0 V and extremes at −0.05 and 0.05 V. In this paper, it is assumed that SCC in Alloy 22 is feasible if the corrosion potential, E_{corr}, exceeds E_{SCC} as defined in Eq. (3).

Based on electrochemical kinetics laws, solving for the potential at which the anodic and cathodic current densities are equal, the following expression for the corrosion potential was derived (see the Appendix A for a detailed derivation):

$$E_{corr} = \frac{E_a^a - E_a^{ef}}{Z_r\beta_r^{ef}F} - \frac{E_a^a}{Z_r\beta_r^{ef}F}\frac{T}{T_{ref}^a} + \frac{RT}{Z_r\beta_r^{ef}F} \times \ln\left[\left(\frac{[H^+]}{1\,mol/L}\right)^{n_H}\left(\frac{pO_2}{1.01\times10^5 Pa}\right)^{n_O}\frac{i_r^{ef}}{i_a^o}\frac{C_{O_2}^{bulk}(T)}{C_{O_2}^{bulk}(T_{ref})}\right], \quad (4)$$

where F is the Faraday constant (9.64867×10^4 C/mol); pO_2, the oxygen partial pressure (2.1×10^4 Pa); R, the ideal gas constant [8.314 J/(mol K)], and $[H^+]$, the concentration of hydrogen ions in mol/L {$[H^+] = -\log_{10}(pH)$}. $C_{O_2}^{bulk}(T)$ is the oxygen concentration in the bulk solution as a function of temperature, and T_{ref} is a reference temperature (298.15 K). $C_{O_2}^{bulk}(T)$ is estimated using an empirical relationship for a pure water system [14]:

$$C_{O_2}^{bulk}(T) = pO_2 e^{-11.228 - \frac{5596.17K}{T} + \frac{1.04967\times10^6 K^2}{T^2}}\frac{mol}{kg\ Pa}. \quad (5)$$

Other variable definitions and values are provided in Table 2. The computed E_{corr}, with the parameters in Table 2, is in units of V_{SHE}. Parameters for Eq. (4) were selected to properly reflect experimental trends of Alloy 22 in a range of temperatures up to 95 °C in full immersion tests. Minimal or no dependencies have been observed between the corrosion potential and the concentration of solutes such as chloride [3]. However, weak dependencies are expected to arise due to oxygen salting out (i.e., reduced concentrations of dissolved oxygen in concentrated salt solutions). Eq. (4) can be modified to account for salting out effects provided there is an available database of the variation of the corrosion potential as a function of dissolved oxygen concentration at fixed temperatures. As a first approximation, such a likely dependence is ignored in this paper.

Experimentally, high values of E_{corr} have been observed when the pH falls below 6 [3]. The transition is due to different kinetics of the cathodic reaction under different pH regimes, as explained in the Appendix A. For the sake of mathematical simplicity, a sharp transition in E_{corr} is assumed to take place at pH 6, although experimentally a more gradual transition is expected. The parameter values to compute E_{corr} for the acidic (pH 6) and alkaline range (pH > 6) are shown in Table 2.

Fig. 1 shows a comparison of values calculated using Eq. (4) to experimental values determined at 95 °C by Dunn et al. [3]. Uncertainty in E_{corr} is assumed to be due to the uncertainty in the anodic current density, i_a^o, associated with the passive dissolution of Alloy 22. The anodic current density is defined via a probability density function (Table 2). The resulting bounds in E_{corr} arising from the consideration of uncertainty in i_a^o are shown in Fig. 1. The i_a^o probability density function was selected so that the median E_{corr} is symmetrically located between upper and low bounds (Fig. 1).

Table 2
Parameters for the computation of the corrosion potential, E_{corr}, as a function of pH and temperature

Parameter	Definition	Value	Value
		pH < 6	pH > 6
E_a^a(kJ/mol)	Effective activation energy for the anodic current density	44.7	44.7
E_a^{ef}(kJ/mol)	Effective activation energy for the cathodic current density	40	40
n_H	Dimensionless constant	0.026	0.019
n_O	Dimensionless constant	0.013	0.025
i_a^o(A/cm^2)	Anodic current density at the reference temperature T_{ref}^a	Sampled from a triangular probability distribution function with extremes at 5×10^{-9} and 2×10^{-8}, and with the maximum (mode) at 6.76×10^{-9}.	
i_r^{ef}(A/cm^2)	Reference cathodic current density	0.024	0.017
T_{ref}^a	Reference temperature for the anodic current density	368.15	368.15
Z_r	Number of electrons in the cathodic reaction	4	4
β_r^{ef}	Effective charge transfer coefficient for the cathodic reaction	0.013	0.025

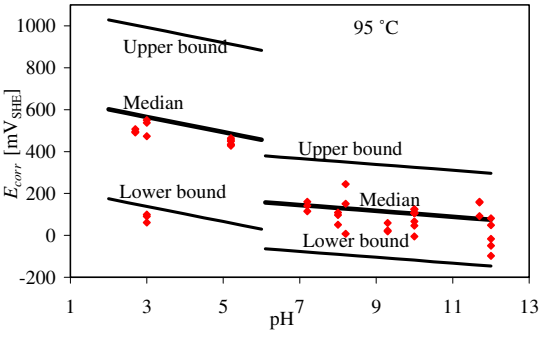

Fig. 1. Comparison of the corrosion potential computed with Eq. (1) to experimental data at 95 °C published in [3].

2.2. Solution compositions

There are three potential sources of water to enable corrosion processes: seepage into the drifts from overlying rocks, condensation due to in-drift cold trap processes, and deliquescence of the salts present in dusts deposited on the waste package surface [15]. In this paper, the source of water of interest is seepage (the other two water sources are not analyzed). Seepage water could contact the waste package if drip shields were breached by some mechanism (e.g., due to rock loads arising from drift degradation and seismic activity). The initial composition of seepage water will evolve over time as a result of evaporation, and concentrated solutions may form that could support the initiation and propagation of CC and SCC. Therefore, this paper further focuses on the analysis of solutions formed by evaporation of seepage waters. The analysis is limited to waste package temperatures up to 110 °C. At rock temperatures well above the water boiling temperature, deep percolating water likely will be diverted away due to the vaporization barrier, making water seepage into the drifts difficult.

The approach to estimate distributions of water compositions is described as follows. The composition of seepage is assumed to be similar to the measured composition of waters in pores of unsaturated zone rock. Thermodynamic simulations of the chemical evolution of in-drift waters resulting from evaporation of porewaters were conducted, using StreamAnalyzer Version 2.0 [16]. The code allows for simulation of aqueous chemical systems for temperatures up to 300 °C, pressures up to 1500 bar, and ionic strengths up to 30 molal. The evaporation simulations were done at 50, 70, 90, and 110 °C. The initial compositions of waters are depicted in the ternary diagram in Fig. 2. The final water vapor pressure was selected as a fraction of the saturation water vapor pressure, with a fraction defined as a function of the waste package temperature (Fig. 3, median value). The range and median value in the water vapor saturation fraction (also referred to as *relative humidity*) as functions of the waste package temperature in Fig. 3 were determined from data from a performance assessment code executed in Monte Carlo mode to account for uncertainty in thermohydrological rock features. This code was used to compute the waste package temperature and relative humidity of air close to the waste package as functions of time, and from these data the median and bounds in Fig. 3 were derived. Uncertainty in the relative humidity at the waste package surface is the result of spatial variability and uncertainty in thermohydrological rock features [17].

The simulations allowed determination of the types of brines that may form in emplacement drifts and the concentration ranges of these brines. The thermodynamic calculations were supplemented by an alternative approach based on the concept of chemical divide developed by Hardie and Eugster [18]. In the chemical divide concept, the chemical types of brines and salt minerals that form upon evaporation of natural waters are determined by early precipitation of insoluble minerals (e.g., calcite and gypsum). Natural waters at Yucca Mountain are considered to evolve into three types of brines upon evaporation: (i) calcium chloride, (ii) neutral, and (iii) alkaline [7]. Thirty-three porewater compositions were used as input to the evaporation simulations selected to represent the broad composition range of the more than 150 samples of Yucca Mountain unsaturated zone porewater reported by Yang et al. [19–21]. To provide a basis for estimating the frequency of

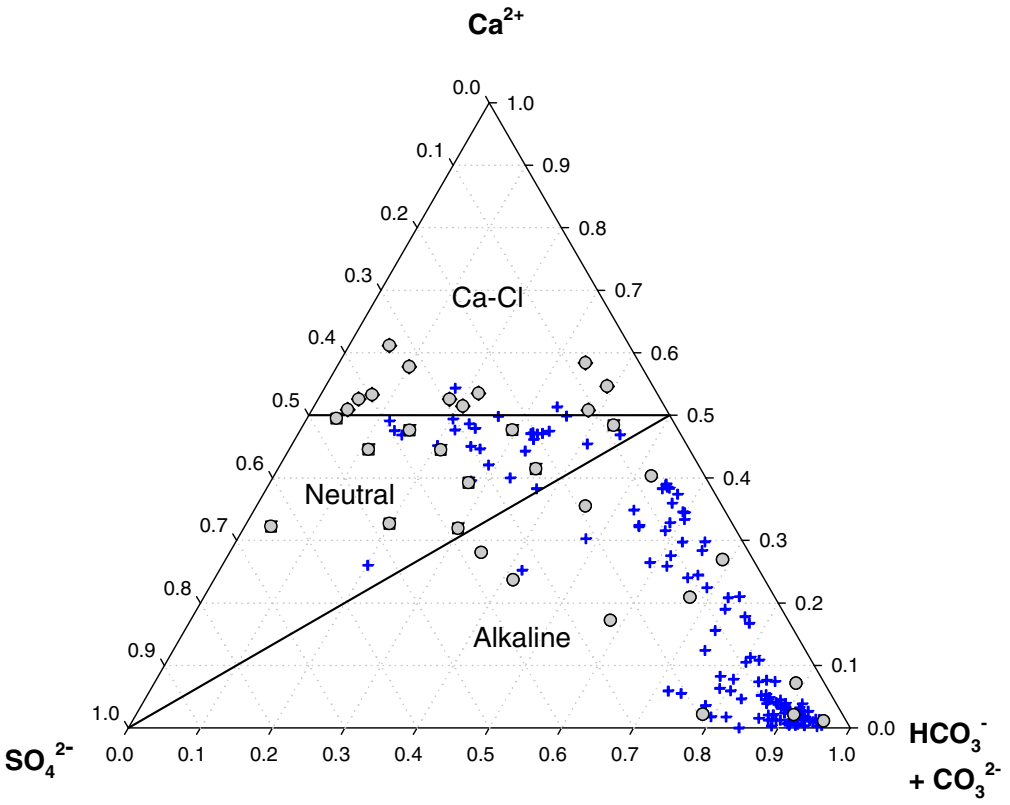

Fig. 2. Compositions of porewaters considered in the thermodynamic simulations (indicated by circles). All of the other data were considered in determining the frequency of the calcium chloride, neutral, or alkaline brines, based on the chemical divide concept. Data are from [19–21].

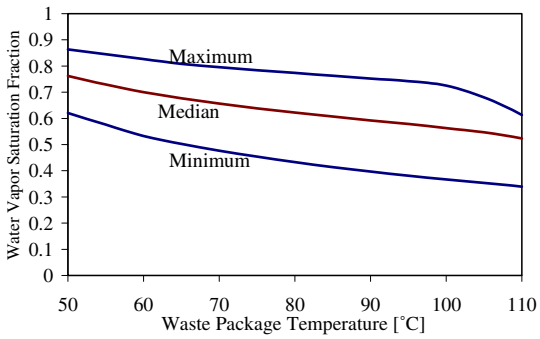

Fig. 3. Values of and uncertainties in the water vapor content in air near the waste package, as a function of temperature.

occurrence of the three brine types and their respective chemical characteristics, the full set of Yang et al. [19–21] data on unsaturated zone porewater compositions was used jointly with the chemical divide concept of Hardie and Eugster [18]. From 156 compositions (all depicted in Fig. 2), 8%, 24%, and 68% resulted into calcium chloride, neutral, and alkaline type brines, respectively. For each of the considered temperatures, distribution functions for pH, $[Cl^-]$, $[NO_3^-]$, $[HCO_3^-]+[CO_3^{2-}]$, and $[SO_4^{2-}]$ were numerically derived by combining the three brine types into a single set, preserving the brine type frequency. The resulting distribution functions were mapped into standard normal distributions (zero mean and unit standard deviation), and covariance matrices of the standardized data were computed (see Appendix B for definitions of standardized mapping and covariance matrix). The computed covariance matrices (with entries rounded to one significant digit) are shown in Table 3. Because diagonal elements of the covariance matrices equal one, covariance and correlation matrices are identical (Appendix B). As expected, at all analyzed temperatures, there is a positive correlation between pH and the total carbonate concentration ($[HCO_3^-]+[CO_3^{2-}]$). In general, the chloride concentration, $[Cl^-]$, is negatively correlated to the oxyanion concentrations, $[NO_3^-]$, $[HCO_3^-]+[CO_3^{2-}]$, and $[SO_4^{2-}]$, due to the salting

Table 3
Covariance[a] matrices of standardized data (data mapped to follow a normal distribution with zero mean and unit standard deviation)

	pH	$[Cl^-]$	$[NO_3^-]$	$[HCO_3^-]+[CO_3^{2-}]$	$[SO_4^{2-}]$
50 °C					
pH	1.0	−0.7	−0.2	0.7	0.3
$[Cl^-]$	−0.7	1.0	−0.3	−0.7	−0.1
$[NO_3^-]$	−0.2	−0.3	1.0	−0.1	−0.4
$[NO_3^-]$, $[HCO_3^-]+[CO_3^{2-}]$	0.7	−0.7	−0.1	1.0	0.4
$[SO_4^{2-}]$	0.3	−0.1	−0.4	0.4	1.0
70 °C					
pH	1.0	−0.5	−0.2	1.0	0.7
$[Cl^-]$	−0.5	1.0	−0.3	−0.6	−0.4
$[NO_3^-]$	−0.2	−0.3	1.0	−0.1	−0.4
$[NO_3^-]$, $[HCO_3^-]+[CO_3^{2-}]$	1.0	−0.6	−0.1	1.0	0.7
$[SO_4^{2-}]$	0.7	−0.4	−0.4	0.7	1.0
90 °C					
pH	1.0	0.0	0.0	0.8	0.5
$[Cl^-]$	0.0	1.0	−0.4	−0.1	0.0
$[NO_3^-]$	0.0	−0.4	1.0	0.0	−0.5
$[NO_3^-]$, $[HCO_3^-]+[CO_3^{2-}]$	0.8	−0.1	0.0	1.0	0.6
$[SO_4^{2-}]$	0.5	0.0	−0.5	0.6	1.0
110 °C					
pH	1.0	−0.2	0.0	0.7	0.2
$[Cl^-]$	−0.2	1.0	−0.5	−0.4	0.2
$[NO_3^-]$	0.0	−0.5	1.0	0.2	−0.8
$[NO_3^-]$, $[HCO_3^-]+[CO_3^{2-}]$	0.7	−0.4	0.2	1.0	0.1
$[SO_4^{2-}]$	0.2	0.2	−0.8	0.1	1.0

[a] Covariance and correlation matrices are identical (Appendix B).

out effect. The magnitude of the correlation coefficient between $[Cl^-]$ and $[NO_3^-]$ increases with increasing temperature. Based on this observation alone, Alloy 22 susceptibility to crevice corrosion, as a function of solution compositions, is higher at higher temperatures. Non-negligible negative correlations between pH and $[Cl^-]$ are noted at the lower temperatures (i.e., at lower temperatures, chloride concentrated solutions are also solutions with low pH).

The numerical cumulative distribution functions (CDF) for pH and the concentration of the various anionic species are shown in Fig. 4 for the various temperatures considered. The pH range tends to increase as the temperature decreases, with a more pronounced temperature dependence on the low end of the pH distribution (Fig. 4(A)). The low bound of the chloride concentration distribution tends to decrease as a function of increasing temperature. Most likely, this behavior is the result of salting out (e.g., as the concentration of other solutes such as nitrate increases with increasing temperature, the chloride solubility decreases). Conversely, the upper range of the chloride concentration distribution is an increasing function of the temperature (Fig. 4(B)). The broader nitrate concentration ranges with increasing temperature are a result of enhanced solubility at higher temperatures (Fig. 4(C)). The total carbonate, $[NO_3^-], [HCO_3^-] + [CO_3^{2-}]$, on the other hand, exhibits retrograde solubility, with higher concentrations at lower temperatures (Fig. 4(D)). The sulfate ion, $[SO_4^{2-}]$, also approximately exhibits some retrograde solubility (higher concentrations are in general associated with the lower temperatures, as in Fig. 4(E)).

The distribution functions in Fig. 4 and the covariance matrices (of standardized data) in Table 3 summarize end compositions after evaporation at various temperatures. To allow for more complete consideration of water composition uncertainty/variability, *feasible* water compositions were constructed by stochastic sampling of the distribution functions in Fig. 4, preserving the covariance matrices in Table 3 (see Appendix B for a detailed explanation of the sampling algorithm). A water composition is a vector of the form {pH, $[Cl^-]$, $[NO_3^-]$, $[HCO_3^-] + [CO_3^{2-}]$, $[SO_4^{2-}]$}. A *feasible* sample of water compositions is a set of vectors such that the numerical cumulative distribution of each vector entry (e.g., pH) is consistent with the distributions in Fig. 4, and the covariance matrix of the standardized set of vectors is consistent with Table 3. By adopting such a stochastic sampling approach, a broader set of water compositions than those arising from the thermodynamic simulations can be considered.

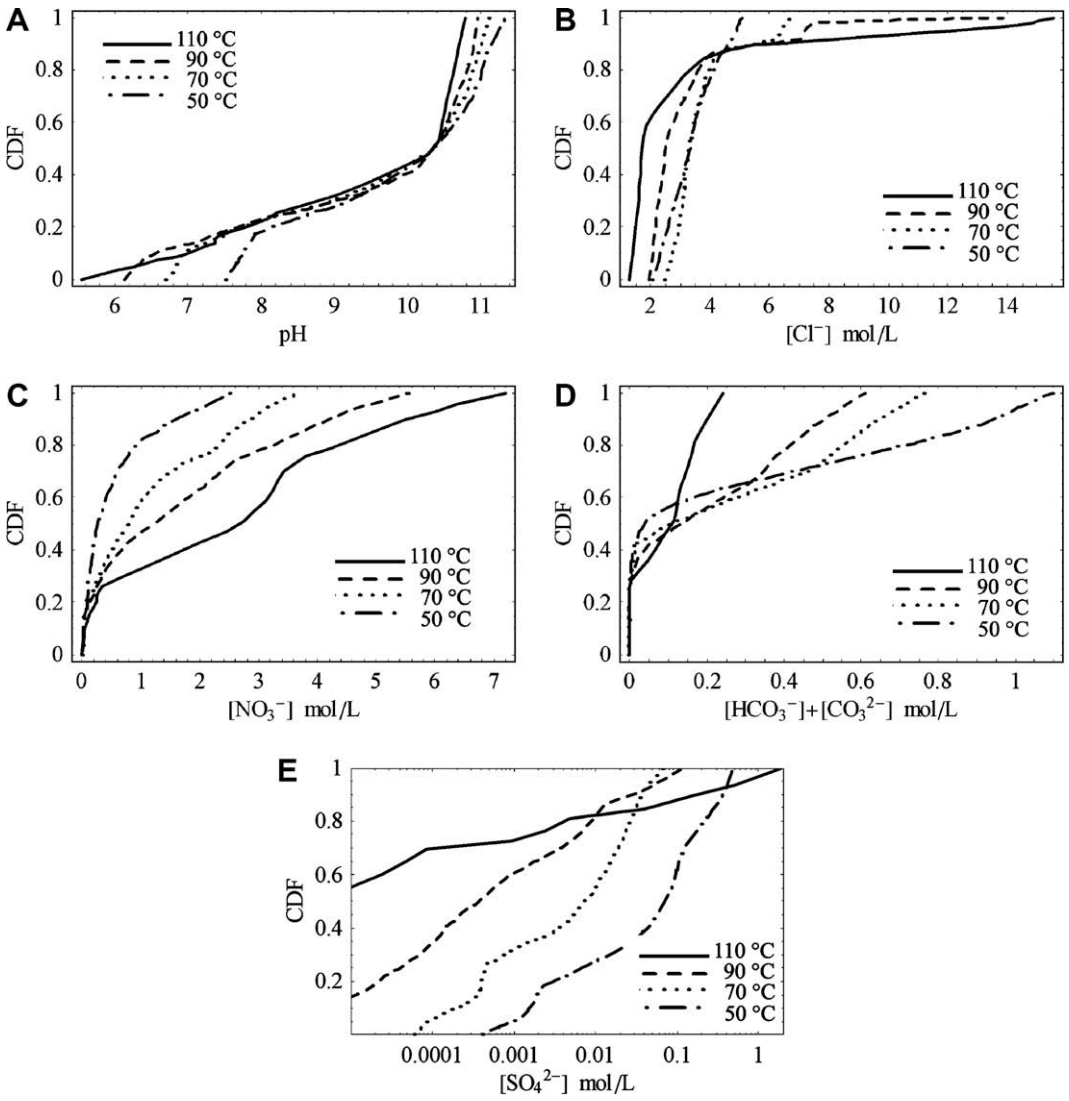

Fig. 4. Cumulative distribution functions (CDF) of chemical components of in-drift waters computed from thermodynamic simulation of evaporation and the chemical divide concept.

2.3. Sampling approach

For each temperature analyzed, a stochastic sample of 10000 feasible water compositions were numerically generated by following the Iman and Conover algorithm to construct correlated samples [22,23] (see Appendix B for details of the Iman and Conover method). This algorithm justifies the adoption of standardized covariance matrices (Table 3), as it accurately reproduces target covariance matrices. For any water composition in the stochastic sample, E_{corr} was computed as a function of pH, the waste package temperature, and the anodic current density (which was sampled from the triangular distribution for i_a^o in Table 1), according to Eq. (4) and parameters in Table 2. For the CC analysis, the repassivation potential, E_{rcrev}, was computed as a function of the temperature and the ionic concentrations $[Cl^-]$, $[NO_3^-]$, $[HCO_3^-] + [CO_3^{2-}]$, and $[SO_4^{2-}]$, according to Eqs. (1) and (2) and parameters in Table 1. Two different values of E_{rcrev} were computed for mill-annealed and thermally aged material (the latter was selected as lower bound for Alloy 22 welds). The uncertainty term ΔE_{rcrev} in Eq. (1) was sampled from triangular distributions defined in Table 1. E_{crit} for SCC, E_{SCC}, was computed according to Eq. (3), with the uncertainty term ΔE_{SCC} sampled from a symmetric triangular distribution spanning from −50 to 50 mV. The fraction of the number of solution compositions satisfying $E_{corr} > E_{crit}$ is an estimator of the probability of the formation of solution compositions capable of promoting the initiation and propagation of CC or SCC, $P(E_{corr} > E_{crit})$.

3. Results and discussion

3.1. Crevice corrosion analysis

Fig. 5 presents scatter plots of $E_{corr} - E_{rcrev}$ for mill-annealed Alloy 22 at 110 °C versus pH and concentrations of the various anionic species. The plots summarize 10000 water compositions, constructed following the stochastic sampling previously described. The fraction of the number of points above the horizontal axis is an estimator of $P(E_{corr} > E_{crit})$ (all of the scatter plots in Fig. 5 include the same number of points above the horizontal axis). In general, the points above the horizontal axis are well spread with respect to pH and the anion concentrations, with the exception of nitrate. In the case of nitrate, $E_{corr} - E_{rcrev} > 0$ only if the nitrate concentration is low. Similar analyses were performed at the other temperatures and for thermally aged material, but the scatter plots

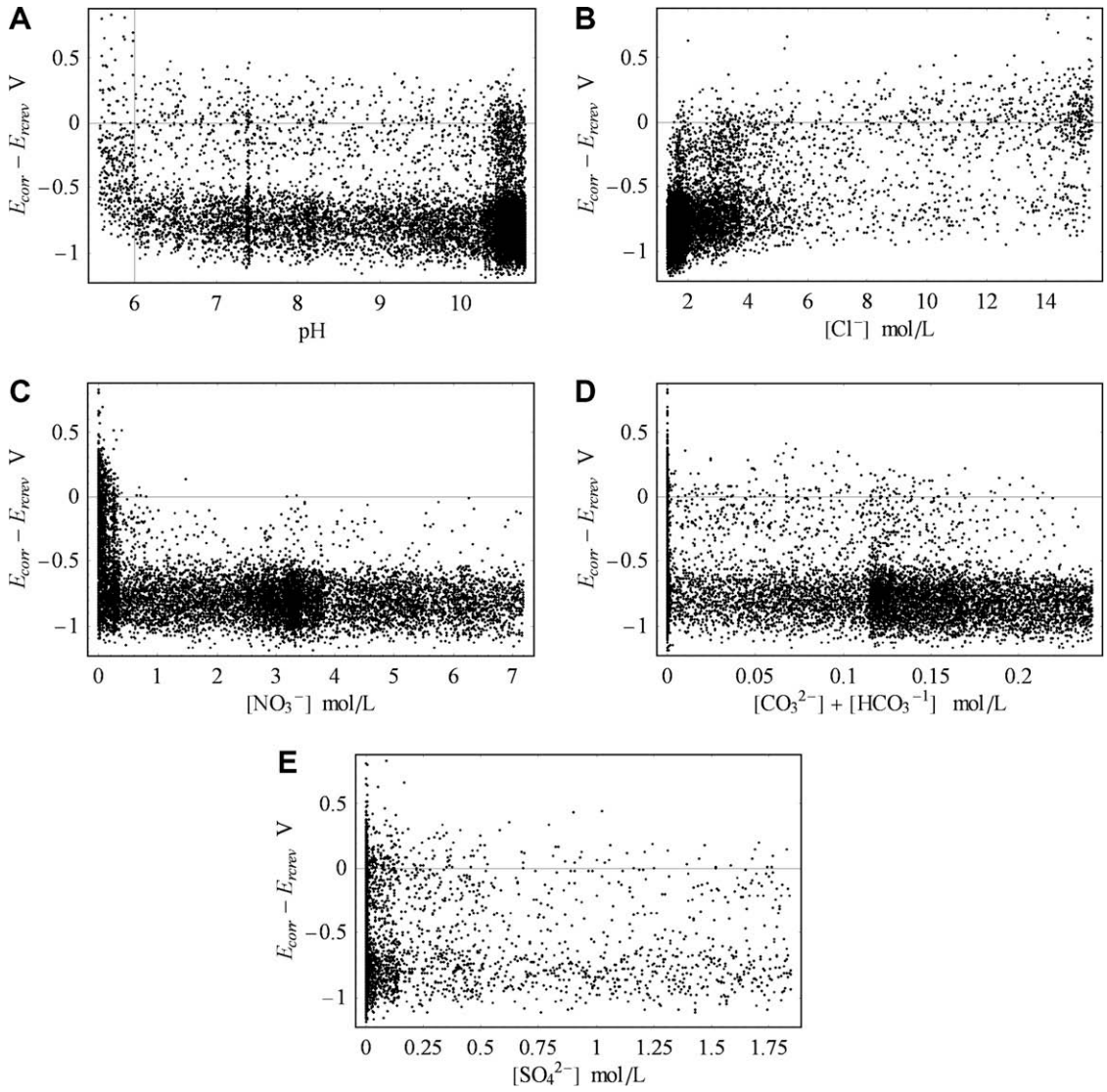

Fig. 5. Scatter plots of the difference $E_{corr} - E_{rcrev}$ versus various chemical components after evaporation of porewaters. The temperature is 110 °C, equations for mill-annealed Alloy 22 were used, and the Monte Carlo mathematical sample included 10^4 points.

are not shown for the sake of brevity. The results are summarized in Fig. 6, indicating the probability of formation of solution compositions capable of promoting the CC initiation.

Fig. 6 shows the fraction of points satisfying $E_{corr} - E_{rcrev} > 0$. Thermally aged material has higher susceptibility to crevice corrosion than mill-annealed material. Fig. 6 indicates that CC is feasible in a range of temperatures. At 50 °C, $P(E_{corr} > E_{rcrev})$ is of the order of 10^{-4} for mill-annealed material, and 0.01 for thermally aged material. At 110 °C, $P(E_{corr} > E_{rcrev})$ is of the order of 0.05 for mill-annealed material and 0.13 for thermally aged material. These probabilities are different compared to those derived from similar computations by Pensado et al. [7] at 110 °C (0.03 and 0.26 for mill-annealed and thermally aged material, respectively). The lower value of $P(E_{corr} > E_{rcrev})$ for thermally aged material in the present analysis is due to (i) updated thermodynamic simulations and (ii) consideration of complete saturation of air with water vapor in Ref. [7] as opposed to partial saturation in the present analysis. Interestingly, lower water vapor saturation leads to more concentrated systems but with higher nitrate concentrations. The higher nitrate-to-chloride ratio in the present analysis is responsible for the lower value of $P(E_{corr} > E_{rcrev})$ for thermally aged Alloy 22 computed at 110 °C compared to the previous evaluation.

The calculated values of $P(E_{corr} > E_{rcrev})$ do not necessarily imply that waste packages in the repository setting could exhibit CC. The condition $E_{corr} > E_{rcrev}$ is only one requirement for CC initiation. Additional requirements must be satisfied for CC to occur, leading to breaching of the waste package and potential release of radionuclides. The probability, P_T, for a waste package to release radionuclides can be computed as

$$P_T = P_S\ P_R\ P\ (E_{corr} > E_{crit})\ P_{WF}, \tag{6}$$

where P_s is the probability for seepage water to contact a waste package; P_R, the probability of formation of appropriate localized corrosion initiation sites (e.g., crevices) including the availability of concentrated solutions at such sites; and P_{WF}, the probability for water to contact and mobilize the waste form in a waste package breached by crevice corrosion. The term P_s is usually computed in performance assessments as a function of scenarios for drip shield failure (e.g., mechanical collapse, general corrosion, hydrogen-induced cracking, and creep). The term P_R has appreciable amounts of uncertainty, depending on the scenario being considered. For example, under a drip shield collapse scenario, crevices could form by contact of the drip shield with the waste package. A concentrated solution must also be available at the crevice site for the initiation of localized corrosion. Recent experimental studies analyzing metal-to-metal crevices indicate a strong dependence of CC initiation on crevice characteristics (e.g., geometry, metal composition) [24]. Crevices could also form on the waste package by contact with the support system in the drifts. The probability P_R should be much smaller for welded regions given that welds may only comprise a small percent of the waste package surface. At this time, a value of P_R has poorly constrained uncertainties, which could be addressed by expert elicitation. It is clear that P_R must be significantly less than one. Focusing on an order of magnitude estimate, a value $P_R \leqslant 0.1$ appears a reasonable selection based on current information. Finally, the term P_{WF} (probability of water contact and mobilization of waste forms in waste packages breached by CC) could be close to one, given the long timeframes of interest. If the waste package is breached by CC, then water likely would continue to be available at the breached location, which would increase the chance for water to infiltrate the waste package. Also, CC breached sites could open as time elapses, increasing the chance for waste forms to be contacted and mobilized by water. Therefore, a value $P_{WF} = 1$ appears reasonable based on current information.

3.2. Stress corrosion cracking analysis

The SCC analysis was slightly different than the CC analysis. In this case, independent analyses were carried out for each of the brine types. Fig. 7 is the cumulative distribution function for the total carbonate in solution, $[HCO_3^-] + [CO_3^{2-}]$, for the three brine types at 110 °C. For SCC to occur, bicarbonate must be present in the solution in sufficient concentration [6,9]. Chiang et al. [6] noted SCC in solutions with bicarbonate concentrations greater than 0.5 molal. From this information, it is inferred that the minimal concentration of bicarbonate needed for SCC may be a fraction of a molar, but the precise threshold value is uncertain at this time. From Fig. 7, assuming 10^{-4} mol/L as threshold value, there is not enough bicarbonate in the calculated calcium chloride brines to support SCC. In the neutral brines, the total carbonate in the system exceeds 10^{-4} mol/L in only a small fraction of the compositions. Only in the calculated alkaline brines there is sufficient concentration of the total carbonate to support SCC in a large proportion of the water compositions. However, as noted in Fig. 1, the corrosion potential decreases with increasing pH and high values of the corrosion potential are also needed for the initiation of SCC [6]. This competition between high corrosion potentials (attainable at low pH) and sufficient bicarbonate concentrations (attainable at high pH) make $E_{corr} > E_{SCC}$ unlikely. Following the mathematical sampling approach previously described, it was estimated $P(E_{corr} > E_{SCC}) = 4 \times 10^{-5}$ for neutral brines and $P(E_{corr} > E_{SCC}) = 5 \times 10^{-5}$ for alkaline brines at 110 °C, assuming a minimal threshold total carbonate value of 10^{-4} mol/L. Considering the 24% and 68% estimated frequency of occurrence for neutral and alkaline brines, respectively, results in a combined average of $P(E_{corr} > E_{SCC}) = 4.8 \times 10^{-5}$ at 110 °C.

As the temperature decreases, SCC is less likely to occur. To derive a notion on the temperature range where SCC is feasible the

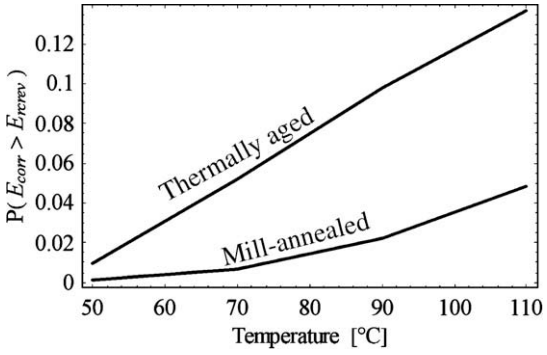

Fig. 6. Fraction of points satisfying $E_{corr} > E_{rcrev}$ as a function of temperature and Alloy 22 metallurgical state.

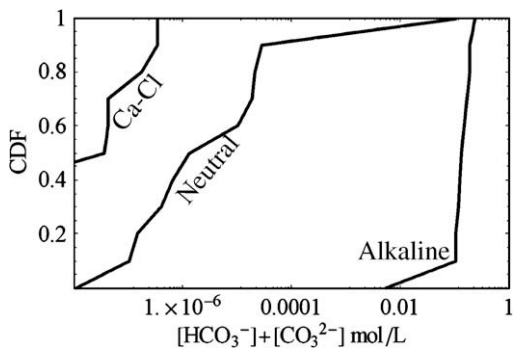

Fig. 7. Cumulative distribution function (CDF) of total carbonate concentration of the three brine types resulting from evaporation of seepage waters at 110 °C.

equation Max(E_{corr}) = Min(E_{SCC}) was examined. Because E_{corr} is a function of pH and temperature and E_{SCC} is, as a first approximation, a function of the temperature only (assuming that bicarbonate and chloride ions are available above minimal concentrations), the equation is satisfied for a set of pH and temperature values. The solution of the equation is presented in Fig. 8. The set of points {T, pH} satisfying Max(E_{corr}) = Min(E_{SCC}) is approximately a straight line with positive slope (Fig. 8). The collection of points {T, pH} below this line defines a region where E_{corr} might exceed E_{crit}. Above the line, SCC is not feasible as $E_{corr} < E_{crit}$. From the thermodynamic simulations at 70, 90, and 110 °C the total carbonate concentration of the brines was less than 10^{-4} mol/L for pH < 9, which is insufficient to promote SCC. The region below the line Max(E_{corr}) = Min(E_{SCC}) and above the line pH 9 defines the region where SCC is feasible (indicated with solid lines in Fig. 8). According to Fig. 8, SCC is unlikely at temperatures less than 100 °C.

A number of uncertainties must be acknowledged that may limit the generality of the conclusions drawn from the present analysis. First, there is uncertainty in the critical potential for SCC. E_{SCC} was determined using a slow strain rate test (SSRT) performed over two weeks using a strain rate of about 2×10^{-6} s^{-1} [6]. The transition between no SCC to SCC appeared smooth as a function of the applied potential in the slow strain rate tests [6]. Therefore, some degree of judgment was unavoidable in determining a threshold value, E_{SCC}, separating tests where SCC was observed from instances where SCC was not. Another source of uncertainty is the possible dependence of E_{SCC} on the strain rate in SSRT. Given that two-week SSRT experiments can only capture SCC with an induction or initiation time shorter than two weeks, it is possible that use of slower strain rates may yield lower values of E_{SCC}. Additional experiments could reduce uncertainties in reported values of E_{SCC}. A second relevant point is the uncertainty in the existence of other solution compositions and systems that may also promote SCC. Using a combinatorial analysis in complex solutions where SCC was known to occur, two principal solution components in the SCC process were identified: chloride and bicarbonate [6]. However, there is no complete certainty that these are the only ions promoting SCC in Alloy 22. These caveats are provided to exercise caution in the use of the information in Fig. 8 and estimated values of $P(E_{corr}>E_{SCC})$.

For abstraction of CC and SCC processes in a performance assessment, an equation equivalent to Eq. (6) can be proposed. The interpretation of the term P_R is slightly different for SCC. It represents the probability of the development of regions of sufficient tensile stress in contact with brines capable of supporting (i.e., initiating and propagating) SCC. Likewise in the CC case, P_R is clearly less than one, but it is highly uncertain and relies on expert judgment. As for the CC case, a value $P_R \leqslant 0.1$ appears reasonable. The fact that $P(E_{corr} > E_{SCC})$ is estimated to be low facilitates simplified

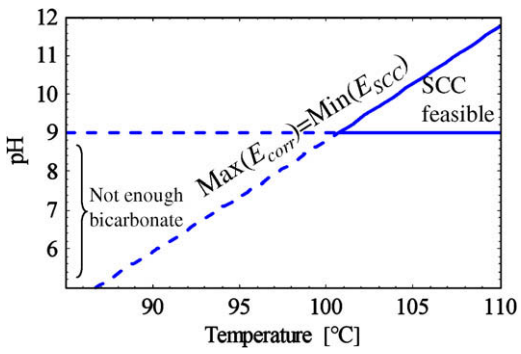

Fig. 8. Plot of temperature and pH showing the feasible region for stress corrosion cracking.

computations for a performance assessment. For example, assuming that each waste package could experience an independent water chemistry, the number of waste packages that could be affected by SCC can be computed as a Poisson distribution with a recurrence rate $\lambda = P_R \times P(E_{corr} > E_{SCC})$; i.e.,

$$P_m = \frac{(\lambda N)^m}{m!} e^{-\lambda N}, \tag{7}$$

where P_m is the probability of m waste packages undergoing SCC and N is the total number of waste packages contacted by seepage water. If $N = 10^4$ and $P_R = 1$, the probability for at least one waste package to undergo SCC is 0.38. If $P_R = 0.1$, the probability is only 0.05. If $P_R = 1$, substitution of $m \geqslant 6$ into Eq. (4) results in $P_m \leqslant 10^{-5}$, which means that it would be unlikely for more than six waste packages to be affected by SCC. In other words, if environmental and material conditions exist for the occurrence of SCC in the repository system, very few waste packages would be affected. Again, the probability values are only provided to demonstrate the use of Eq. (7). Some caution should be exercised in using these numbers given the uncertainties previously discussed.

4. Conclusions

An approach was developed to assess the likelihood of environmental conditions capable of supporting (i.e., initiating and propagating) CC or SCC of an Alloy 22 waste package in potential repository aqueous environments. The approach was based on thermodynamic simulations of evaporation of porewaters and published equations to compute corrosion potential, E_{corr}, and critical potentials, E_{crit}, for CC and SCC as functions of pH, ionic concentration, temperature, and waste package fabrication states. From probability distribution functions for solution compositions and covariance matrices derived from thermodynamic simulations, the probability for E_{corr} to exceed E_{crit}, P($E_{corr} > E_{crit}$), was estimated for both CC and SCC. The probability $P(E_{corr} > E_{rcrev})$ was defined as a function of Alloy 22 metallurgical states from waste package fabrication processes (mill-annealed or thermally aged) in the CC analysis. It was found that $P(E_{corr} > E_{rcrev})$ for CC ranges from a few percent to 13% for temperatures ranging from 50 to 110 °C. To support performance assessments, an approach to estimate the percentage of waste packages breached by CC and contributing to radionuclide release was proposed, that depends on definition of additional conditional probabilities related to the likelihood of the formation of crevices conducive to localized corrosion. With respect to SCC, the analysis suggested that SCC is a process that is feasible, but unlikely, at temperatures above the boiling point of pure water. SCC is unlikely due to competing requirements of sufficient bicarbonate concentrations and high corrosion potentials. Uncertainties, which were acknowledged in the analysis, could be addressed with additional experimental studies on SCC. Examples are presented to show how the approach might be used in system-level assessment of repository performance.

Acknowledgements

The authors want to thank G.A. Cragnolino for technical discussions during the development of this work and reviews by S. Mohanty, X. He, and L. Mulverhill. This paper was prepared to document work performed by the CNWRA for the US Nuclear Regulatory Commission (NRC) under Contract No. NRC–02–07–006. The activities reported here were performed on behalf of the NRC Office of Nuclear Material Safety and Safeguards, Division of High-Level Waste Repository Safety. This paper is an independent product of the CNWRA and does not necessarily reflect the view or regulatory position of the NRC.

Appendix A. Corrosion potential equation

Symbols

$C_{O_2}^{bulk}(T)$	oxygen concentration in solution at temperature T, mol/kg
E_a^a	effective activation energy for the anodic current density, J/mol
E_a^o	activation energy for the reference cathodic current density, J/mol
E_a^{ef}	effective activation energy, J/mol
E_{corr}	corrosion potential, V
F	Faraday constant, 9.64867×10^4 C/mol
i_a^o	anodic current density at the temperature T_{ref}^a, A/m^2
i_r^{ef}	positive constant, A/m^2
i_r^{ref}	reference cathodic current density, A/m^2
i_r^o	oxygen reduction current density, A/m^2
n_H, n_O	dimensionless constants
pO_2	partial pressure of oxygen over the solution, Pa
R	ideal gas constant, 8.314 J/(mol K)
T	temperature, K
T_{ref}	reference temperature, 298.15 K
T_{ref}^a	reference temperature for anodic current density, 368.15 K
Z_r	number of electrons in the fundamental charge transfer reaction, 4
α_E, α_H, α_O	dimensionless constants
β_r	charge transfer coefficient, dimensionless
β_r^{ef}	effective charge transfer coefficient, dimensionless
$\phi_{f/s}$	potential drop at the film-solution interface, V
$\phi_{f/s}^o$	constant potential, V
$[H^+]$	hydrogen ion concentration, mol/L

This appendix shows a detailed derivation of the equation to compute the corrosion potential, Eq. (4). The likely dominant cathodic reaction under oxidizing conditions and neutral to alkaline pH is

$$O_2 + 2H_2O + 4e^- \rightarrow 4OH^-. \tag{A.1}$$

Assuming a first order reaction with respect to oxygen and ignoring activity coefficient corrections and backward reactions, the contribution to the cathodic current density from oxygen reduction, i_r^o, as a function of temperature and potential at the oxide-solution interface can be computed from

$$i_r^o = -i_r^{ref} e^{-\frac{E_a^o}{R}\left(\frac{1}{T}-\frac{1}{T_{ref}}\right)} \frac{C_{O_2}^{bulk}(T)}{C_{O_2}^{bulk}(T_{ref})} e^{-\frac{Z_r\beta_r F}{RT}\phi_{f/s}}. \tag{A.2}$$

Eq. (A.2) is a variant of the Butler–Volmer equation [25], written in the form suggested by Macdonald [26] with explicit reference to the potential drop at the oxide film–solution interface, $\phi_{f/s}$, as opposed to the system overpotential. The minus sign next to the term i_r^{ref} represents the convention that cathodic current densities are defined as negative and anodic current densities as positive. The concentration of oxygen in solution, $C_{O_2}^{bulk}(T)$, is defined as Eq. (5).

Consistent with the theory of oxide films by Macdonald [26], the potential drop, $\phi_{f/s}$, is assumed to be a linear function of the corrosion potential, E_{corr}:

$$\phi_{f/s} = \alpha_E E_{corr} - \alpha_H \frac{RT}{F}\log_{10}\left(\frac{\{[H^+]}{1\text{mol/L}}\right) - \alpha_O \times \frac{RT}{F}\log_{10}\left(\frac{pO_2}{1.01\times 10^5\text{Pa}}\right) + \phi_{f/s}^o. \tag{A.3}$$

Macdonald's [26] original equation for the potential drop at the film solution interface, $\phi_{f/s}$, was generalized by including a term that is dependent on the partial pressure of oxygen in air, pO_2, and on the temperature. The constants in the denominators in the parentheses, 1 mol/L and 1.01×10^5 Pa (=1 atm), are included in the equation for the sake of dimensional consistency and to define a reference state. After combining Eqs. (A.2) and (A.3), the expression for the partial cathodic current density becomes

$$i_r^o = -i_r^{ef} \times \frac{C_{O_2}^{bulk}(T)}{C_{O_2}^{bulk}(T_{ref})} e^{-\frac{E_a^{ef}}{RT}} e^{-\frac{Z_r\beta_r^{ef}F}{RT}E_{corr}} \left(\frac{[H^+]}{1}\text{mol/L}\right)^{n_H} \left(\frac{pO_2}{1.01\times 10^5\text{Pa}}\right)^{n_O}. \tag{A.4}$$

The terms i_r^{ef}, E_a^{ef}, β_r^{ef}, n_H, and n_O are defined as functions of more fundamental terms from Eqs. (A.2) and (A.3), but explicit definitions are omitted in this appendix for brevity. The term β_r^{ef} is such that $0 < \beta_r^{ef} < 1$. The constants i_r^{ef} and E_a^{ef} are both positive, while n_H and n_O could have any value. These terms were estimated by fitting computed values of the corrosion potential to empirical data.

Eq. (A.4) is valid for neutral to alkaline solutions. Under acidic conditions, a reaction likely to dominate the cathodic current density is

$$O_2 + 4H^+ + 4e^- \rightarrow 2H_2O. \tag{A.5}$$

Following the derivation previously described, an expression of identical form to Eq. (A.4) can be derived for the cathodic current density associated with reaction (A.5). However, the corresponding terms i_r^{ef}, E_a^{ef}, β_r^{ef}, n_H, and n_O have different values in the acidic regime (see Table 2 for estimated values in alkaline and acidic regimes).

The anodic current density, i_a, due to passive dissolution of Alloy 22, is computed according to

$$i_a(T) = i_a^o e^{-\frac{E_a^a}{R}\left(\frac{1}{T}-\frac{1}{T_{ref}^a}\right)}. \tag{A.6}$$

The anodic current density is defined independently of the corrosion potential, consistent with empirical observations indicating a weak dependence in the passive regime [27,3]. Based on passive current densities measured potentiostatically over periods longer than two weeks, an Arrhenius dependence of the passive current density on temperature has been verified [3].

The corrosion potential, E_{corr}, is defined as the potential at which the total current density $[i_a(T) + i_r^o(T)]$ equals zero. Solving for this requirement, the following equation is derived

$$E_{corr} = \frac{E_a^a - E_a^{ef}}{Z_r\beta_r^{ef}F} - \frac{E_a^a}{Z_r\beta_r^{ef}F}\frac{T}{T_{ref}^a} + \frac{RT}{Z_r\beta_r^{ef}F} \times \ln\left[\left(\frac{[H^+]}{1\text{mol/L}}\right)^{n_H}\left(\frac{pO_2}{1.01\times 10^5\text{Pa}}\right)^{n_O}\frac{i_r^{ef}}{i_a^o}\frac{C_{O_2}^{bulk}(T)}{C_{O_2}^{bulk}(T_{ref})}\right], \tag{A.7}$$

which is the same as Eq. (1). Fig. 1 in this paper shows a comparison of the corrosion potential computed using Eq. (A.7) to data in [3]. Uncertainty in the corrosion potential is assumed to be dominated by the uncertainty in the reference anodic current density, i_a^o.

Appendix B. Statistical Definitions and Correlated Sampling Algorithm

Sample

A random variable is denoted with a single-subscript symbol, x_j. The symbol c_j denotes the cumulative distribution function of x_j. For example, x_j could represent pH or any of the anionic species ($[Cl^-]$, $[NO_3^-]$, $[HCO_3^-] + [CO_3^{2-}]$, or $[SO_4^{2-}]$). The function c_j is depicted in Fig. 4. A *sample* of variable x_j is a set

$$\mathbf{x}_j = \{x_{1j}, x_{2j}, \ldots, x_{nj}\}^T, \tag{B.1}$$

with entries x_{ij} following the distribution function c_j. The superscript T is the transpose operator; used to denote the convention that $\mathbf{x}_j$ is a column vector. The sample size, n, in this paper is 10^4.

Standard normal mapping

The set $\mathbf{y}_j = \{y_{1j}, y_{2j}, \cdots, y_{nj}\}^T$ is the *standard normal mapping* of $\mathbf{x}_j$ if each entry, y_{ij}, is computed as

$$y_{ij} = \sqrt{2} erf^{-1}(2c_j(x_{ij}) - 1). \tag{B.2}$$

The error function is erf and its inverse is erf^{-1}. The set $\mathbf{y}_j$ follows a *standard normal distribution* (zero mean and unit standard deviation).

Covariance matrix

Let $\{x_1, x_2, x_3, \ldots, x_v\}$ be a set of variables –for example, {pH, $[Cl^-]$, $[NO_3^-]$, $[HCO_3^-] + [CO_3^{2-}]$, $[SO_4^{2-}]$}– and $\mathbf{X}$ be the total sample matrix:

$$\mathbf{X} = \begin{pmatrix} x_{11} & x_{12} & \cdots & x_{1v} \\ x_{21} & x_{22} & \cdots & x_{2v} \\ \vdots & \vdots & \vdots & \vdots \\ x_{n1} & x_{n2} & \cdots & x_{nv}. \end{pmatrix} \tag{B.3}$$

The sample $\mathbf{x}_j$ (representing variable x_j) is the jth column of $\mathbf{X}$. If $\{x_1, x_2, x_3, \ldots, x_v\}$ is {pH, $[Cl^-]$, $[NO_3^-]$, $[HCO_3^-] + [CO_3^{2-}]$, $[SO_4^{2-}]$}, then a *solution composition* is a row of $\mathbf{X}$.

The mean m_j of the sample $\mathbf{x}_j$ is

$$m_j = \frac{1}{n}\sum_{i=1}^{n} x_{ij}. \tag{B.4}$$

The mean matrix, $\mathbf{M}$, of the sample $\mathbf{X}$ is defined as

$$\mathbf{M} = \begin{pmatrix} m_1 & m_2 & \cdots & m_v \\ m_1 & m_2 & \cdots & m_v \\ \vdots & \vdots & \vdots & \vdots \\ m_1 & m_1 & \cdots & m_v \end{pmatrix}_{n\times v}. \tag{B.5}$$

The *covariance matrix*, $\mathrm{Cov}(\mathbf{X}) = \mathbf{C}_X$, is defined as

$$\mathrm{Cov}(\mathbf{X}) = \mathbf{C}_\mathbf{X} = \frac{1}{n}(\mathbf{X} - \mathbf{M})^T(\mathbf{X} - \mathbf{M}). \tag{B.6}$$

Some authors consider $n-1$ as opposed to n as the denominator of the covariance matrix to distinguish from a maximum-likelihood covariance. Because the value of n is usually large ($n = 10^4$ in this paper), such distinction is not significant. $\mathbf{C}_X$ is a symmetric matrix of dimension $v \times v$.

Correlation matrix

If C_{ij} is the (i, j) entry of the covariance matrix $\mathbf{C}$, then the correlation matrix $\mathbf{R}$ is defined as a matrix with entries R_{ij} equal to

$$R_{ij} = \frac{C_{ij}}{\sqrt{C_{ii}}\sqrt{C_{jj}}}, \tag{B.7}$$

C_{ii} and C_{jj} are diagonal entries of $\mathbf{C}$. If each diagonal element of $\mathbf{C}$ equals one, covariance and correlation matrices are identical.

Correlated sampling algorithm

The correlated sampling method employed in this paper is based on the Iman and Conover algorithm [22]. The algorithm is based on the observation that if a sample $\mathbf{Z}$ is defined as

$$\mathbf{Z} = \mathbf{XA} \tag{B.8}$$

($\mathbf{A}$ is any matrix of dimension $v \times v$) then the covariance matrix, $\mathrm{Cov}(\mathbf{Z})$, is

$$\mathrm{Cov}(\mathbf{Z}) = \mathbf{A}^T Cov(\mathbf{X})\mathbf{A} \tag{B.9}$$

Eq. (B.9) can be directly verified by applying the definitions in Eqs. (B.4), (B.5), and (B.6) to the matrix $\mathbf{Z} = \mathbf{X}\,\mathbf{A}$.

Because $\mathbf{C}$ is a symmetric matrix, by the eigen decomposition theorem [28], $\mathbf{C}$ can be expressed as

$$\mathbf{C} = \mathbf{EDE}^T \tag{B.10}$$

$\mathbf{E}$ is an orthogonal matrix; i.e.,

$$\mathbf{EE}^T = \mathbf{E}^T\mathbf{E} = \mathbf{I}, \tag{B.11}$$

$\mathbf{D}$ is a diagonal matrix with the positive eigenvalues, and $\mathbf{I}$, the identity matrix. The eigenvalues are necessarily positive because $\mathbf{C}$ is defined as the product of a matrix and its transpose, Eq. (B.6). Let the eigenvalues (diagonal entries on the matrix $\mathbf{D}$) be symbolized as λ_j^2 ($j = 1, 2, \ldots, v$), and let the matrix Λ be a diagonal matrix with λ_j ($j = 1, 2, \ldots, v$) as the diagonal entries. If the matrix $\mathbf{Q}$ is defined as

$$\mathbf{Q} = \mathbf{E}\Lambda. \tag{B.12}$$

It can be directly verified that

$$\mathbf{C} = \mathbf{QQ}^T \tag{B.13}$$

The decomposition of $\mathbf{C} = \mathbf{Q}\,\mathbf{Q}^T$ is an important step in the Iman and Conover algorithm [22]. These authors considered the Cholesky decomposition algorithm [28] to express $\mathbf{C}$ as the product of a matrix and its transpose. Eigen and Cholesky decomposition algorithms are available in standard mathematical software such as *Mathematica*® [29].

Assume $\mathbf{U}$ is a matrix of size $n \times v$, with entries u_{ij} computed as

$$u_{ij} = \sqrt{2} erf^{-1}(2p_{ij} - 1) \tag{B.14}$$

where p_{ij} is a uniform random number in the open interval (0, 1). Entries in a column of $\mathbf{U}$ follow a standard normal distribution.

If $\mathbf{C}_U = \mathrm{Cov}(\mathbf{U})$ and $\mathbf{C}_U = \mathbf{Q}_U\mathbf{Q}_U^T$ [Eq. (B.13)], then the sample constructed as

$$\tilde{\mathbf{U}} = \mathbf{U}(\mathbf{Q}_\mathbf{U}^T)^{-1} \tag{B.15}$$

satisfies

$$\mathrm{Cov}(\tilde{\mathbf{U}}) = \mathbf{Q}_\mathbf{U}^{-1}\mathbf{C}_\mathbf{U}(\mathbf{Q}_\mathbf{U}^T)^{-1} = \mathbf{I} \tag{B.16}$$

Let $\mathbf{C}_t$ be a target covariance matrix (e.g., one of the matrices in Table 3) and $\mathbf{C}_t$ be decomposed as

$$\mathbf{C}_t = \mathbf{Q}_{\mathbf{C}_t}\mathbf{Q}_{\mathbf{C}_t}^T. \tag{B.17}$$

If the sample $\mathbf{Y}$ is

$$\mathbf{Y} = \tilde{\mathbf{U}}\mathbf{Q}_{\mathbf{C}_t}^T = \mathbf{U}\left(\mathbf{Q}_\mathbf{U}^T\right)^{-1}\mathbf{Q}_{\mathbf{C}_t}^T \tag{B.18}$$

then $\mathrm{Cov}(\mathbf{Y}) = \mathbf{C}_t$:

$$\mathrm{Cov}(\mathbf{Y}) = \mathbf{Q}_{\mathbf{C}_t}\mathrm{Cov}(\tilde{\mathbf{U}})\mathbf{Q}_{\mathbf{C}_t}^T = \mathbf{Q}_{\mathbf{C}_t}\mathbf{Q}_{\mathbf{C}_t}^T = \mathbf{C}_t. \tag{B.19}$$

Therefore, a random sample, $\mathbf{Y}$, constructed as defined in Eq. (B.18), has a covariance matrix identical to the target covariance, $\mathbf{C}_t$.

Entries on a column of $\mathbf{Y}$ necessarily follow a normal distribution with zero mean. If the diagonal elements of the target covariance, $\mathbf{C}_t$, equal 1, then the standard deviation of entries in any column is also 1 (i.e., columns of $\mathbf{Y}$ follow the standard normal distribution). In that particular case, to construct a sample in the x-variable space, the following mapping can be applied

$$x_{ij} = c_j^{-1}\left(\frac{1}{2} + \frac{1}{2} erf\left(\frac{y_{ij}}{\sqrt{2}}\right)\right) \quad \text{(B.20)}$$

y_{ij} is the (i, j) entry of the sample matrix **Y**. A sample $\mathbf{x}_j$ ($j = 1, 2, \ldots, v$) thus constructed follows the c_j distribution function. If the total sample **X** is standardized according to Eq. (B.2), the covariance matrix of the standardized sample, **Y**, equals $\mathbf{C}_t$.

Feasible water composition

In this paper, samples **X** with $n = 10^4$ elements were constructed according to the algorithm described here (the variables represented were {pH, $[Cl^-]$, $[NO_3^-]$, $[HCO_3^-] + [CO_3^{2-}]$, $[SO_4^{2-}]$}) so that the matrix, Cov(**Y**), would equal a covariance matrix from Table 3. Any row of **X** is referred to as a *feasible water composition*.

References

[1] F. Hua, G. Gordon, Corrosion 60 (2004) 764.
[2] J.A. Rard, K.J. Staggs, S.D. Day, S.A. Carroll, J. Solut. Chem. 35 (2006) 1187.
[3] D.S. Dunn, O. Pensado, Y.-M. Pan, L. Yang, X. He, in: P. Van Isheghem (Ed.), Scientific Basis for Nuclear Waste Management XXIX, Mat. Res. Soc. Symp. Proc. 932, Warrendale, Pennsylvania, 2006, p. 853.
[4] D.S. Dunn, Y.-M. Pan, L. Yang, G.A. Cragnolino, Corrosion 61 (2005) 1078.
[5] D.S. Dunn, Y.-M. Pan, L. Yang, G.A. Cragnolino, Corrosion 62 (2006) 3.
[6] K.T. Chiang, D.S. Dunn, G.A. Cragnolino, Corrosion 63 (2007) 940.
[7] O. Pensado, R. Pabalan, D. Dunn, K.-T. Chiang, in: P. Marcus, V. Maurice (Eds.), Passivation of Metals and Semiconductors, and Properties of Thin Oxide Layers – A Selection of Papers from the Ninth International Symposium, Paris, France, 27 June – 1 July 2005, Elsevier, The Netherlands, 2006, p. 53.
[8] D.S. Dunn, L. Yang, C. Wu, G.A. Cragnolino, in: J.M. Hanchar, S. Stroes-Gascoyne, L. Browning (Eds.), Scientific Basis for Nuclear Waste Management XXVIII, Mat. Res. Soc. Symp. Proc. 824, Warrendale, Pennsylvania, 2004, p. 33.
[9] P.K. Shukla, D.S. Dunn, K.T. Chiang, O. Pensado, Stress Corrosion Cracking Model for Alloy 22 in the Potential Yucca Mountain Repository Environment, CORROSION 2006, paper 06502, NACE International, Houston, Texas, 2006.
[10] M.C. Reheis, Dust Deposition in Nevada, California, and Utah, 1984–2002, Open-file Report 03-138, US Geological Survey, 2003.
[11] Z.E. Peterman, T.A. Oliver, in: D.S. Dunn, C. Poinssot, B. Begg (Eds.), Materials Research Society Symposium on the Scientific Basis for Nuclear Waste Management XXX, Mat. Res. Soc. Symp. Proc. 985, Warrendale, Pennsylvania, 2007, p. 541.
[12] D.S. Dunn, G.A. Cragnolino, N. Sridhar, Corrosion 56 (2000) 90.
[13] A. Anderko, N. Sridhar, D.S. Dunn, Corros. Sci. 46 (2004) 1583.
[14] R. Batino (Ed.), International Union of Pure and Applied Chemistry (IUPAC) Solubility Data Series: Oxygen and Ozone, Pergamon, New York, 1981, p. 7.
[15] L. Browning, R. Fedors, L. Yang, O. Pensado, R. Pabalan, C. Manepally, B. Leslie, in: J.M. Hanchar, S. Stroes-Gascoyne, L. Browning (Eds.), Scientific Basis for Nuclear Waste Management XXVIII, Mat. Res. Soc. Symp. Proc. 824, Warrendale, Pennsylvania, 2004, p. 417.
[16] OLI Systems, Inc., A Guide to Using the OLI Software for version 2.0 of the Analyzers, OLI Systems Inc., Morris Plains, New Jersey, 2005.
[17] C. Manepally, R. Fedors, in: Proceedings of the 10th International High-Level Radioactive Waste Management Conference, Las Vegas, Nevada, 30 March–3 April, 2003 (Published in CD-ROM), American Nuclear Society, La Grange Park, Illinois, 2003.
[18] L.A. Hardie, H.P. Eugster, Evolution of Closed-basin Brines, Mineralogical Society of America, Special Paper No. 3, 1970, p. 273.
[19] I.C. Yang, Z.E. Peterman, K.M. Scofield, J. Contam. Hydrol. 62&63 (2003) 361.
[20] I.C. Yang, P. Yu, G.W. Rattray, J.S. Ferarese, J.N. Ryan, US Geological Survey Water-Resources Investigations Report 98-4132, Denver, Colorado, 1998.
[21] I.C. Yang, G.W. Rattray, Y. Pei, US Geological Survey Water-Resources Investigations Report 96-4058, Denver, Colorado, 1996.
[22] R.L. Iman, W.J. Conover, Commun. Stat.: Simul. Comput. B11 (1982) 311.
[23] J.C. Helton, Reliab. Eng. Syst. Safety 42 (1993) 327.
[24] X. He, D.S. Dunn, A.A. Csontos, Electrochim. Acta 52 (2007) 7556.
[25] J.O'M. Bockris, A.K.N. Reddy, Modern Electrochemistry, vol. 2, Plenum Publishing Corporation, New York, 1970.
[26] D.D. Macdonald, J. Electrochem. Soc. 139 (1992) 3434.
[27] D.S. Dunn, C.S. Brossia, in: CORROSION 2002, paper 02548, NACE International, Houston, Texas, 2002.
[28] W.H. Press, S.A. Teukolsky, W.T. Vetterling, B.P. Flannery, Numerical Recipes in FORTRAN: The Art of Scientific Computing, Second., Cambridge University Press, Cambridge, England, UK, 1992.
[29] Wolfram Research, Inc., Mathematica, Wolfram Research, Inc., Champaign, Illinois, <www.wolfram.com>, 2008.